ELSEVIER

Materials Science and Engineering A 476 (2008) 316–321

MATERIALS SCIENCE & ENGINEERING A

www.elsevier.com/locate/msea

# Martensitic transformation of annealed $Ti_{50}Ni_{25}Cu_{25}$ melt-spun ribbons

S.H. Chang [a], S.K. Wu [a,b,*], H. Kimura [c]

[a] *Department of Materials Science and Engineering, National Taiwan University, Taipei 106, Taiwan*
[b] *Department of Mechanical Engineering, National Taiwan University, Taipei 106, Taiwan*
[c] *Institute for Materials Research, Tohoku University, Sendai 980-8577, Japan*

Received 25 February 2007; received in revised form 26 April 2007; accepted 26 April 2007

**Abstract**

Martensitic transformation of annealed melt-spun $Ti_{50}Ni_{25}Cu_{25}$ ribbons is investigated. Experimental results reveal that $Ti_{50}Ni_{25}Cu_{25}$ ribbons annealed at a temperature above or below $T_x$ have identical crystallization behavior and exhibit B2 ↔ B19 martensitic transformation. $Ti_{50}Ni_{25}Cu_{25}$ ribbons can have good shape memory effect and damping capacity when annealed under appropriate conditions to acquire abundant crystallized grains with low Cu content. In order to obtain the optimal shape memory effect, it is better to anneal crystallized ribbons at temperature between $T_g$ and $T_x$ because crystallization of ribbons is slower and it is easier to control their properties.


*Keywords:* Shape memory alloys (SMA); Martensitic phase transformation; Amorphous materials; Shape memory effect; Internal friction

## 1. Introduction

TiNi-based alloys exhibiting thermolelastic martensitic transformation are known to be the most important shape memory alloys (SMAs) with excellent shape memory effect (SME) and superelasticity [1]. Substituting Cu for Ni in the Ti–Ni binary SMAs has been known to lower the transformation hysteresis, the superelasticity hysteresis, and the flow stress level in the martensite state [2,3]. The transformation sequences of $Ti_{50}Ni_{50-x}Cu_x$ SMAs are B2 ↔ B19′, B2 ↔ B19 ↔ B19′ and B2 ↔ B19 for $x<5$, $5\leq x\leq 20$ and $x>20$ at.%, respectively [3–5]. Here, B2 is parent phase, B19 and B19′ are orthorhombic and monoclinic martensite, respectively. It was found that Cu addition exceeding 10 at.% in $Ti_{50}Ni_{50-x}Cu_x$ SMAs seriously embrittles and reduces the alloy's workability, and thus restrains the practical applications of high Cu-content Ti–Ni–Cu SMAs [3,6]. In recent years, melt-spinning techniques have been utilized to fabricate high Cu-content Ti–Ni–Cu ternary SMAs in order to avoid their intrinsic restriction of workability. $Ti_{50}Ni_{25}Cu_{25}$ ribbon has been widely studied because of its small transformation hysteresis, large transformation strain, and one-stage B2 ↔ B19 transformation [7–16]. The as-spun $Ti_{50}Ni_{25}Cu_{25}$ ribbons fabricated using a high cooling rate in the melt-spinning process are completely amorphous and show no SME. Therefore, a proper thermal annealing is required to crystallize the as-spun amorphous ribbons to achieve a good SME. Several articles have reported the effect of annealing condition on the microstructure, texture, martensitic transformation and shape memory property [17–20]. However, up to now, the annealing effects on the martensitic transformation behavior of the crystallized $Ti_{50}Ni_{25}Cu_{25}$ melt-spun ribbons have not been elucidated in detail. In this study, $Ti_{50}Ni_{25}Cu_{25}$ melt-spun ribbons are annealed to crystallize at three different temperatures for differing time intervals. Two of the annealing temperatures are chosen between glass transition temperature ($T_g$) and crystallization temperature ($T_x$) and the other is chosen at a temperature above $T_x$. Thereafter, the effects of annealing on martensitic transformation, SME and damping characteristic of the annealed ribbons are studied by differential scanning calorimetry (DSC) and dynamic mechanical analyzer (DMA).

## 2. Experimental procedures

The $Ti_{50}Ni_{25}Cu_{25}$ amorphous ribbons used in this study were prepared by the Institute for Materials Research, Tohoku University, Sendai, Japan, using a single-roller melt-spinning technique. The detailed procedure for specimen preparation

* Corresponding author at: Department of Materials Science and Engineering, National Taiwan University, Taipei 106, Taiwan. Tel.: +886 2 2363 7846; fax: +886 2 2363 4562.
*E-mail address:* skw@ntu.edu.tw (S.K. Wu).

0921-5093/$ – see front matter © 2007 Elsevier B.V. All rights reserved.
doi:10.1016/j.msea.2007.04.102

and the amorphous characteristics of the as-spun $Ti_{50}Ni_{25}Cu_{25}$ ribbons are described elsewhere [16]. The as-spun ribbon was first cut into test specimens and heated at a constant heating rate of 20 °C/min from room temperature to 550 °C using DSC equipment (TA DSC 2000) to determine its $T_g$ and $T_x$ temperatures. For specimens annealed at temperatures between $T_g$ and $T_x$, the as-spun ribbons were annealed at 435 °C and 450 °C by TA DSC 2000 in a nitrogen atmosphere. Here, $Ti_{50}Ni_{25}Cu_{25}$ amorphous specimen was first heated and equilibrated at 400 °C and then heated again to 435 °C or 450 °C at a constant rate of 10 °C/min. Thereafter, the specimen was kept isothermally at 435 °C or 450 °C for a certain time interval and then promptly removed from the DSC cell followed by quenching in water. For the ribbons annealed at a temperature above $T_x$, the as-spun ribbons were sealed in evacuated quartz tubes and annealed at 500 °C in a salt bath for different time intervals and subsequently quenched in water. Transformation temperatures of the aforementioned annealed specimens were determined by TA Q10 DSC with a heating/cooling rate of 10 °C/min. The shape recoverable strains of the annealed specimens were measured by the tensile test under a constant stress of 90 MPa using a film tension clamp of TA 2980 DMA with a heating/cooling rate of 3 °C/min. The damping characteristics of the annealed specimens were also investigated by TA 2980 DMA with the same heating/cooling rate (3 °C/min). The amplitude and frequency employed were 10 μm (strain amplitude = $1.2 \times 10^{-3}$) and 10 Hz, respectively. Microstructure observations and composition analysis for the annealed ribbons were performed using a Philips XL 30 scanning electron microscopy (SEM) equipped with an energy dispersive spectrometry (EDS). The EDS results are the average of at least five tests in similar places. The ribbons for microstructure observations were sealed in evacuated quartz tubes and annealed at 450 °C in a salt bath for different time intervals followed by quenching in water to avoid the formation of oxide layer during the annealing process. Thereafter, the annealed ribbons were etched by the solution of $HClO_3$: $CH_3COOH$ = 5:100 in volume ratio.

## 3. Experimental results

### 3.1. DSC results of amorphous and annealed $Ti_{50}Ni_{25}Cu_{25}$ ribbons

Fig. 1(a) shows the DSC heating curve of the as-spun amorphous ribbon measured at a constant heating rate of 20 °C/min. As shown in Fig. 1(a), a $T_g$ temperature at 400 °C and a $T_x$ temperature at 460 °C can be detected. Obviously, there is an extended supercooled liquid region between $T_g$ and $T_x$. Hence, the isothermal annealing temperatures are chosen at 435 °C, 450 °C and 500 °C. Fig. 1(b) plots the DSC curves of the as-spun amorphous ribbons isothermal annealed at 435 °C and 450 °C. In Fig. 1(b), both DSC curves show a single exothermic peak after a certain period of incubation time. Moreover, as shown in Fig. 1(b), the incubation time is shorter and the crystallization process is faster when the ribbon is annealed at a higher temperature. Fig. 2(a–c) shows the DSC cooling curves of the ribbons annealed at 435 °C, 450 °C and 500 °C, respectively, for

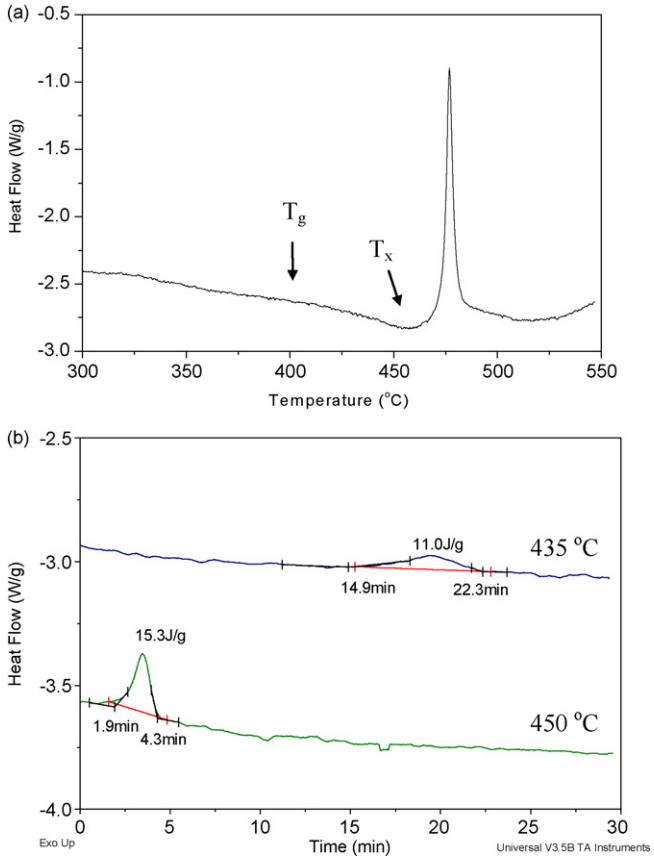


Fig. 1. (a) DSC curve of as-spun $Ti_{50}Ni_{25}Cu_{25}$ ribbon measured at a constant heating rate of 20 °C/min and (b) the isothermal DSC curves of the as-spun $Ti_{50}Ni_{25}Cu_{25}$ ribbon measured at isothermal annealing temperatures of 435 °C and 450 °C.

different time intervals. As seen in Fig. 2, all specimens exhibit an asymmetric peak shape of B2 → B19 martensitic transformation upon cooling, i.e., sharp from the high-temperature side and smooth from the low-temperature one. This phenomenon is associated with the fact that the stored elastic energy associated with martensitic transformation increases with increase in volume fraction of the martensite and retards the forward transformation. Similar behavior has been observed in $Ni_{42.5}Mn_{50}Ti_{7.5}$ [21] and $Ti_{40.5}Ni_{49.5}Zr_{10}$ [22] SMAs.

### 3.2. DMA results of annealed $Ti_{50}Ni_{25}Cu_{25}$ ribbons

Fig. 3(a–c) shows the DMA strain–temperature curves of $Ti_{50}Ni_{25}Cu_{25}$ melt-spun ribbons annealed at 435 °C, 450 °C and 500 °C, respectively, for different time intervals. In Fig. 3, the tensile stress employed is 90 MPa, which is low enough to forbid the retained strain following the thermal cycling test. As illustrated in Fig. 3, the annealed melt-spun ribbons exhibit a well-defined shape recovery upon complete crystallization of the ribbons. Among them, the crystallized ribbons annealed at 435 °C, 450 °C and 500 °C for 30 min, 10 min and 3 min, respectively, exhibit the maximum shape recoverable strain of about 2.2%, 2.3% and 2.0%. Fig. 4(a) shows the DMA tan δ and storage modulus $E_0$ curves of $Ti_{50}Ni_{25}Cu_{25}$ melt-spun ribbons annealed at 500 °C for 3 min. In Fig. 4(a), for the tan δ curve, a B2 → B19

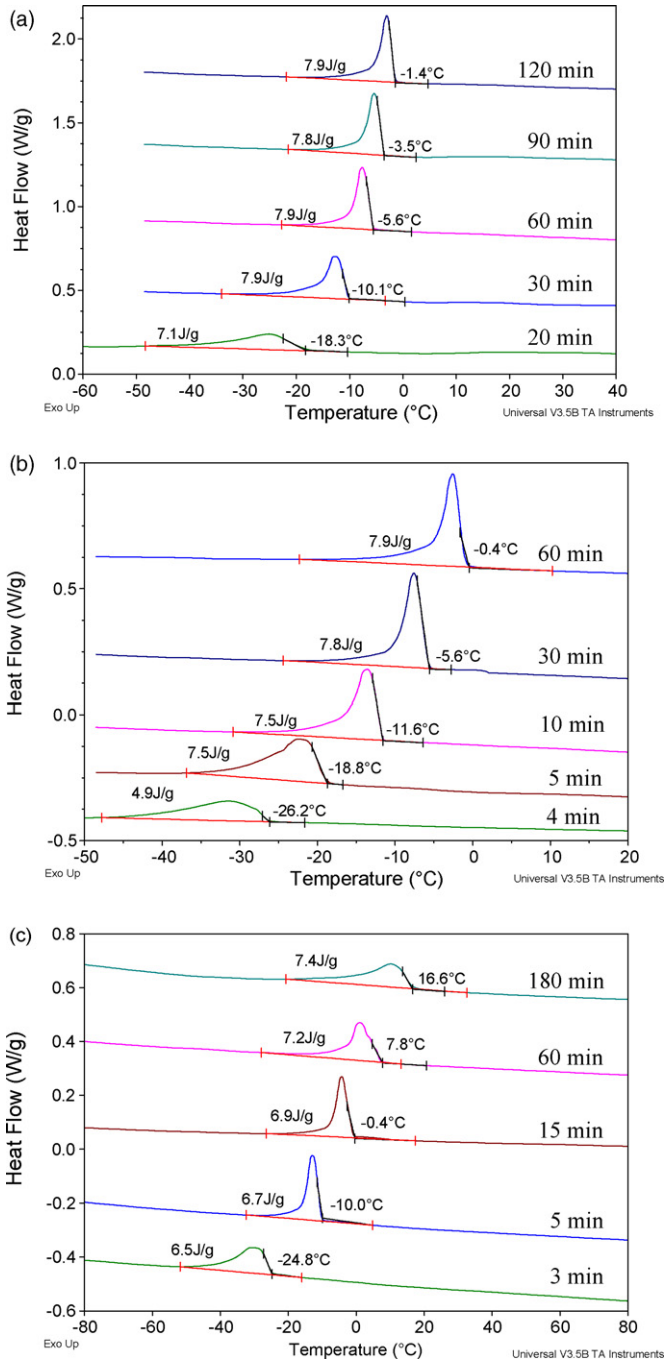


Fig. 2. DSC curves of $Ti_{50}Ni_{25}Cu_{25}$ ribbon annealed at (a) 435 °C, (b) 450 °C and (c) 500 °C for different time intervals.

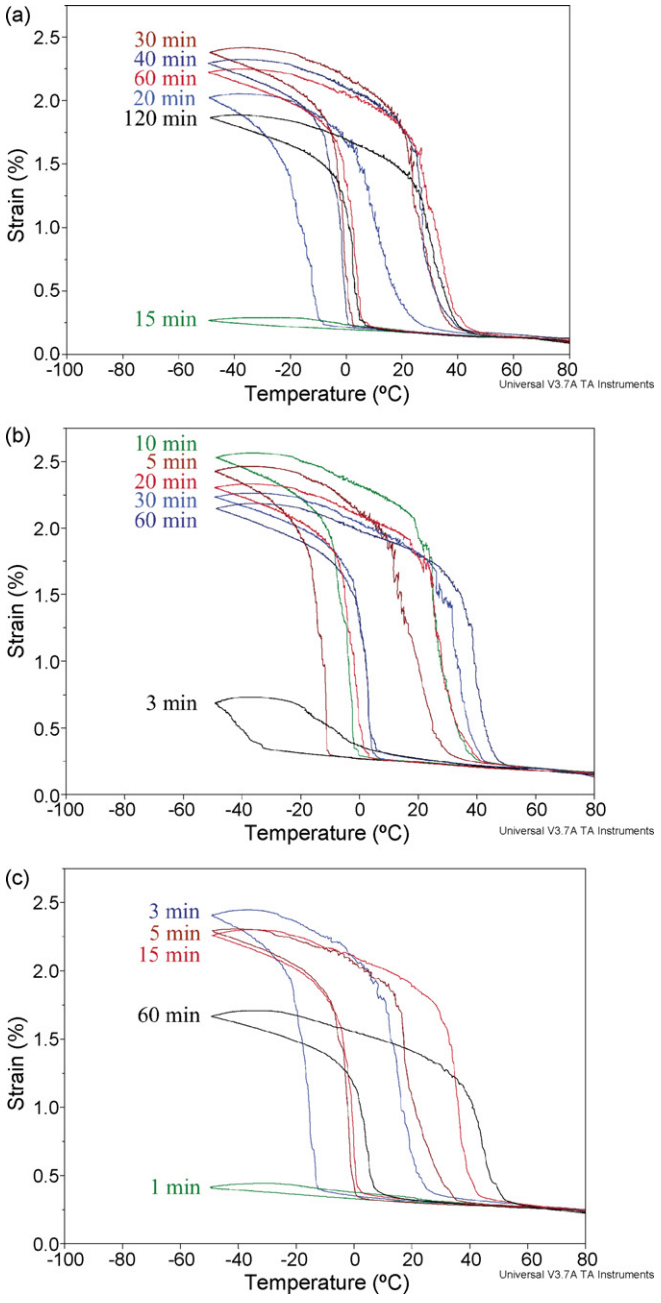


Fig. 3. DMA tensile curves for $Ti_{50}Ni_{25}Cu_{25}$ ribbon annealed at (a) 435 °C, (b) 450 °C and (c) 500 °C for different time intervals.

transformation peak and an extra broadening peak are observed at about −20 °C and −75 °C, respectively. The extra peak at −75 °C is known as a relaxation peak which is not observed in the DSC curve [23]. Moreover, from Fig. 4(a), the measured $E_0$ curve declines gently in the B2 parent phase while cooling, and drops significantly during B2 → B19 transformation. After B2 → B19 transformation is completed, the $E_0$ value of B19 martensite increases quickly with a decrease in temperature. Fig. 4(b) shows the tan $\delta$ curves of the ribbons annealed at 500 °C for different time intervals. As illustrated in Fig. 4(b), the specimen annealed for 3 min has the highest tan $\delta$ transformation peak and relaxation peak with the former having its tan $\delta$ value of 0.07. When the annealing time is prolonged, both transformation peak and relaxation peak shift gradually to high temperatures but their tan $\delta$ values decrease simultaneously. Moreover, as shown in Fig. 4(b), the ribbon annealed at 500 °C for 1 min possesses a very low tan $\delta$ value and exhibits neither a transformation peak nor relaxation peak.

### 3.3. SEM results of anneale d $Ti_{50}Ni_{25}Cu_{25}$ ribbons

Fig. 5(a–c) shows the SEM micrographs of ribbons annealed at 450 °C for 3 min, 10 min and 60 min, respectively. The results of EDS analyses for chemical compositions of points 1–6 are

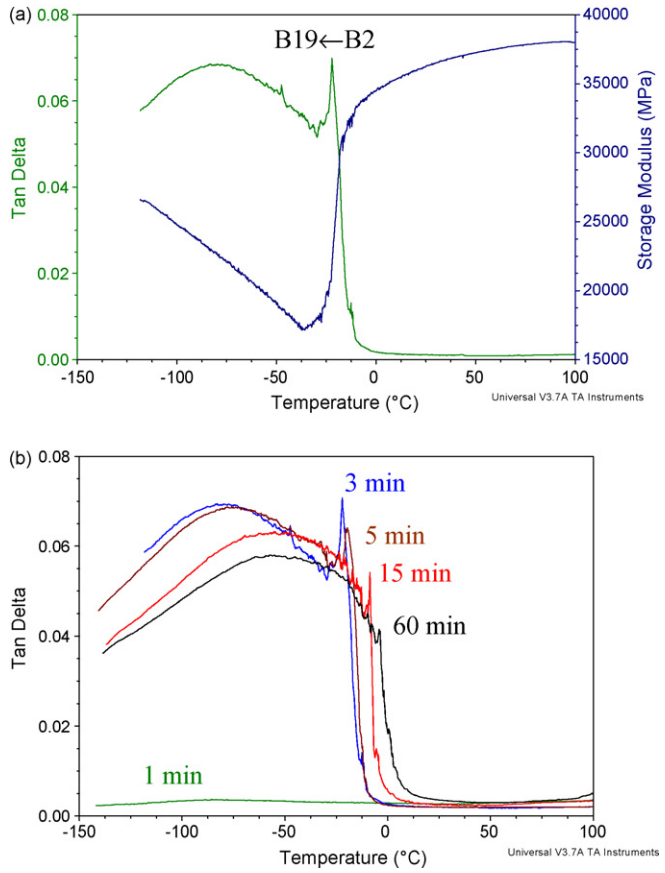


Fig. 4. (a) DMA tan $\delta$ and $E_0$ curves of $Ti_{50}Ni_{25}Cu_{25}$ ribbon annealed at 500 °C for 3 min and (b) DMA tan $\delta$ curves of $Ti_{50}Ni_{25}Cu_{25}$ ribbons annealed at 500 °C for different time intervals.

also denoted in Fig. 5. In Fig. 5(a), when the specimen is annealed at 450 °C for 3 min, only about 40% of the area has been crystallized in the amorphous matrix with the grain sizes of 1–3 μm. Obviously, at this annealing condition, the crystallization process is not completed. Moreover, the crystallized grains (point 1) contain a higher Ti content and a lower Cu content of about 51.74 at.% and 21.51 at.%, respectively, than those of the amorphous matrix (point 2). For ribbons annealed at 450 °C for 10 min, as shown in Fig. 5(b), more crystallized grains are developed and their grain sizes increase to about 4–6 μm. The Ti content of the crystallized grains (point 3) decreases to 51.29 at.% while the Cu content increases to 24.04 at.%. Comparing Fig. 5(b) with (a) reveals that the decreasing Ti content and the increasing Cu content in crystallized grains are due to the diffusion of Ti and Cu atoms between the matrix and the crystallized grains. After annealing at 450 °C for 60 min, as shown in Fig. 5(c), the crystallized area and grains size are almost similar to those in Fig. 5(b). This indicates that the fraction of the crystallized area and the sizes of the crystallized grains do not increase conspicuously with further annealing upon complete crystallization. At the same time, as illustrated in Fig. 5(c), the Ti and Cu contents in crystallized grains (point 5) decrease continuously to 50.07 at.% and increase to 24.84 at.%, respectively, and are close to those in the matrix (point 6). This is because Ti and Cu atoms diffuse continuously between the matrix and the crystallized grain, and thus the chemical composition throughout the ribbon eventually approaches equilibrium after sufficient annealing. The tendency of the evolution in microstructure and the change in composition of the ribbons annealed at 500 °C are similar to those shown in Fig. 5 [16]. This feature indicates that the crystallization behavior is similar when ribbons are annealed at temperatures above or below $T_x$.

## 4. Discussion

### 4.1. Martensitic transformation of annealed $Ti_{50}Ni_{25}Cu_{25}$ ribbons

Fig. 6(a) plots the specimen's $\Delta H_c$ values of Fig. 2 as a function of annealing time. For ribbons annealed at 435 °C and 450 °C, the measured $\Delta H_c$ value is low when the crystallization is incomplete, such as annealing at 435 °C and 450 °C for 19 min and 4 min, respectively. For ribbons annealed at 500 °C, on the other hand, the low $\Delta H_c$ value is not obtained because the crystallization process is too rapid. Upon prolonging the annealing time, the $\Delta H_c$ value of the ribbons annealed at 435 °C and 450 °C increases and eventually reaches 8.0 J/g, and that annealed at 500 °C eventually approaches 7.5 J/g. In Fig. 6(a), the low $\Delta H_c$ value at the beginning of the annealing time is due to the insufficient crystallization of the annealed ribbons, as shown in Fig. 5(a). Upon complete crystallization, the $\Delta H_c$ values almost remain constant because the fraction of the crys-

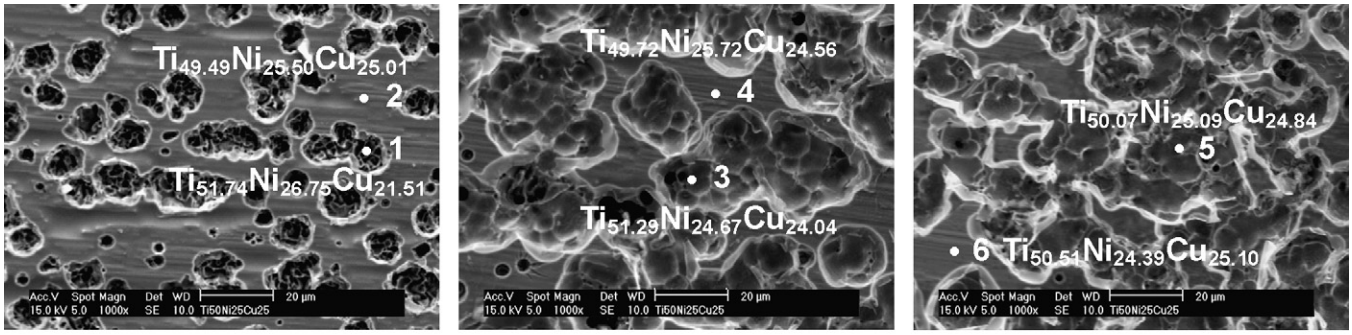


Fig. 5. SEM micrographs and EDS analyses of $Ti_{50}Ni_{25}Cu_{25}$ ribbon annealed at 450 °C for (a) 3 min, (b) 10 min and (c) 60 min.

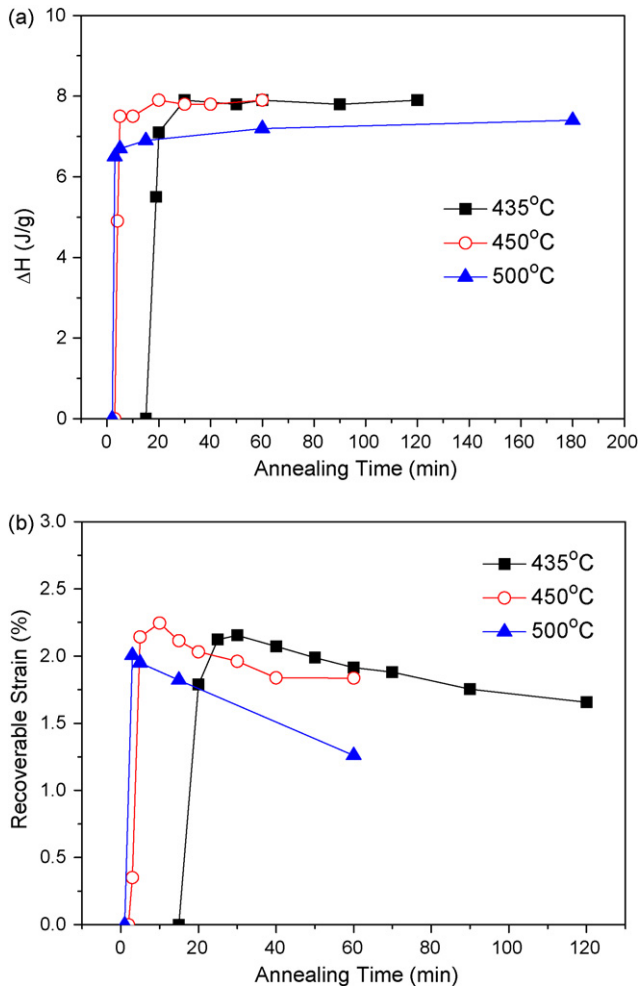


Fig. 6. Changes of the (a) $\Delta H_c$ and (b) shape recoverable strain of $Ti_{50}Ni_{25}Cu_{25}$ ribbons annealed at 435 °C, 450 °C and 500 °C as a function of annealing time.

tallized area and the size of the crystallized grains do not increase conspicuously, as shown in Fig. 5(b and c).

Fig. 6(b) plots the specimen's shape recoverable strain measured from Fig. 3 as a function of annealing time. From Figs. 4(b) and 6(b), when the ribbon is incompletely crystallized, such as the specimens annealed at 435 °C, 450 °C and 500 °C for less than 20 min, 5 min and 1 min, respectively, no obvious martensitic transformation and thus no SME or sharp damping capacity can be obtained. When ribbons are annealed at 435 °C, 450 °C and 500 °C for 30 min, 10 min and 3 min, respectively, as shown in Fig. 6(b), crystallized ribbons exhibit maximum shape recoverable strains. Meanwhile, for specimen annealed at 500 °C for 3 min, as shown in Fig. 4(b), its transformation peak and relaxation peak also exhibit the greatest $\tan\delta$ values. These features are closely related to the fact that there are abundant crystallized grains developed in the annealed ribbons when the crystallization is finished, as shown in Fig. 5(b). However, from Figs. 4(b) and 6(b), both the shape recoverable strain and the $\tan\delta$ value of crystallized ribbons decrease with further increase in annealing time. Liu and co-workers [18–20] proposed that formation of excessive B11-TiCu precipitates and the texture development deteriorate the shape memory and thermomechanical properties of the crystallized $Ti_{50}Ni_{25}Cu_{25}$ ribbons when they are annealed at temperature above 550 °C. In addition, it has also been reported that $Ti_{50}Ni_{25}Cu_{25}$ ribbons can form precipitates when they are annealed at high temperature (e.g., above 550 °C) or for extremely long interval (e.g., 48 h at 410 °C) [7,10–12]. Therefore, precipitate formation and texture effect do not account for the decreasing shape recoverable strain and $\tan\delta$ value because the annealing temperatures and time intervals employed in this study are much lower than 550 °C and 48 h, respectively. Since the fraction of the crystallized area and the $\Delta H_c$ value of the annealed ribbons are almost the same after crystallization of ribbons is complete, the decreasing shape recoverable strain and $\tan\delta$ value are not attributable to the change in the crystallized area, but are mainly because of the alteration in composition in the crystallized grains. Nam et al. [3] reported that the maximum recoverable elongation associated with B2 ↔ B19 transformation decreases with increasing Cu content in bulk $Ti_{50}Ni_{50-x}Cu_x$ SMAs. Therefore, the aforementioned decreasing shape recoverable strain and $\tan\delta$ value of the crystallized ribbons can be attributed to the increasing Cu content in the crystallized grains.

### 4.2. Annealing temperature effect

Experimental results of Figs. 3–6 reveal that the annealing condition influences significantly the SME and damping characteristics of crystallized $Ti_{50}Ni_{25}Cu_{25}$ ribbons. This annealing effect is similar whether the ribbons are annealed at a temperature above or below $T_x$. However, as shown in Fig. 6(b), if the specimens are annealed at 500 °C (above $T_x$), only the specimen annealed for 3 min can possess a good shape recoverable strain, say 2.0%. On the other hand, for ribbons annealed at temperatures between $T_g$ and $T_x$, the specimens annealed at 435 °C for 25–40 min and those at 450 °C for 5–15 min can all possess shape recoverable strain of above 2.0%. In other words, the ribbons annealed at a lower temperature can acquire good SME over a wider annealing time interval upon complete crystallization. This is because the higher the annealing temperature, the faster the atoms diffuse in between the matrix and crystallized grains, and thus the SME of annealed ribbons deteriorates more rapidly. Consequently, from the viewpoint of shape memory applications of melt-spun $Ti_{50}Ni_{25}Cu_{25}$ ribbons, we expect that the ribbons can possess high shape recoverable strain and good damping capacity by appropriate control of the annealing conditions. Since the effect of annealing on the crystallization behavior and thus the SME of the crystallized ribbons is similar regardless whether the ribbons are annealed at a temperature above or below $T_x$, it is preferable to choose the annealing temperature between $T_g$ and $T_x$ because it is easier to control the annealing condition to obtain higher SME and damping capacity of the crystallized ribbons.

## 5. Conclusions

In this study, martensitic transformation of melt-spun $Ti_{50}Ni_{25}Cu_{25}$ ribbons annealed at temperatures above and below

$T_x$ for different time intervals is investigated by DSC and DMA tests. Experimental results reveal that shape memory effect and damping capacity of crystallized $Ti_{50}Ni_{25}Cu_{25}$ melt-spun ribbons are significantly influenced by the annealing condition. When the ribbon is incompletely crystallized, no sharp damping capacity and no good SME can be obtained because no obvious martensitic transformation occurred in the ribbon. The crystallized $Ti_{50}Ni_{25}Cu_{25}$ ribbon exhibits its maximum shape recoverable strain and the highest tan $\delta$ value when its crystallization process is just completed. This is because, at this time, there are abundant crystallized grains with the lowest Cu content in the crystallized ribbons. Both shape recoverable strain and tan $\delta$ value of the ribbon deteriorate with further prolonged annealing due to the increasing Cu and decreasing Ti content in the crystallized grains. Consequently, in view of the shape memory applications of melt-spun $Ti_{50}Ni_{25}Cu_{25}$ ribbons, it is preferable to choose the annealing temperature between $T_g$ and $T_x$ because it is easier to control the annealing condition to acquire abundant crystallized grains with lower Cu content, and thus to obtain better SME and damping capacity of the crystallized ribbons.

## Acknowledgements

The authors gratefully acknowledge the financial support of the National Science Council (NSC), Taiwan, Republic of China, under the Grant NSC95-2221-E002-163. We also sincerely acknowledge Dr. Ho-Sou Chen, a fellow of American Physical Society, who assisted the ribbons preparation and guided the investigation in this study.

## References

[1] C.M. Wayman, T.W. During, in: T.W. During, K.N. Melton, D. Stöckel, C.M. Wayman (Eds.), Engineering Aspects of Shape Memory Alloys, Butterworth-Heinemam, London, 1990, pp. 3–20.
[2] Y.C. Lo, S.K. Wu, H.E. Horng, Acta Metall. Mater. 41 (1993) 747.
[3] T.H. Nam, T. Saburi, K. Shimizu, Mater. Trans., JIM 31 (1990) 959.
[4] T.H. Nam, T. Saburi, Y. Nakata, K. Shimizu, Mater. Trans., JIM 31 (1990) 1050.
[5] H. Miyamoto, T. Taniwaki, T. Ohba, K. Otsuka, S. Nishigori, K. Kato, Scripta Mater. 53 (2005) 171.
[6] S. Miyazaki, K. Mizukoshi, T. Ueki, T. Sakuma, Y.N. Liu, Mater. Sci. Eng. A 273–275 (1999) 658.
[7] H. Rösner, P. Schloβmacher, A.V. Shelyakov, A.M. Glezer, Acta Mater. 49 (2001) 1541.
[8] Z.L. Xie, J. Van Humbeek, Y. Liu, L. Delaey, Scripta Mater. 37 (1997) 363.
[9] H. Rösner, A.V. Shelyakov, A.M. Glezer, K. Feit, P. Schloβmacher, Mater. Sci. Eng. A 273–275 (1999) 733.
[10] C. Satto, A. Ledda, P. Potapov, J.F. Janssens, D. Schryvers, Intermetallics 9 (2001) 395.
[11] R. Santamarta, D. Schryvers, Mater. Trans. 44 (2003) 1760.
[12] R. Santamarta, E. Cesari, J. Pons, T. Goryczka, Metall. Mater. Trans. 35A (2004) 761.
[13] Y. Liu, Mater. Sci. Eng. A 354 (2003) 286.
[14] G.P. Cheng, Z.L. Xie, J. Alloys Compd. 396 (2005) 128.
[15] S.H. Chang, S.K. Wu, H. Kimura, Mater. Trans. 47 (2006) 2489.
[16] S.H. Chang, S.K. Wu, H. Kimura, Intermetallics 15 (2007) 233.
[17] G.P. Cheng, Z.L. Xie, Y. Liu, J. Alloys Compd. 415 (2006) 182.
[18] G.P. Cheng, Z.L. Xie, Y. Liu, Mater. Sci. Eng. A 425 (2006) 268.
[19] Y. Liu, Z.L. Xie, Y.X. Tong, C.W. Lim, J. Alloys Compd. 416 (2006) 188.
[20] Z.L. Xie, G.P. Cheng, Y. Liu, Acta Mater. 55 (2007) 361.
[21] P.L. Potapov, R. Gotthardt, L. Bataillard, Phys. Status Solidi 165 (1998) 401.
[22] S.F. Hsieh, S.K. Wu, J. Alloys Compd. 403 (2005) 154.
[23] S.K. Wu, H.C. Lin, T.S. Chou, Mater. Trans. 47 (2006) 711.